Structural Abnormalities in the Papillary and Peripapillary Areas and Corresponding Visual Field Defects in Eyes With Pathologic Myopia

Shiqi Xie, Koju Kamoi, Tae Igarashi-Yokoi, Kengo Uramoto, Hiroyuki Takahashi, Noriko Nakao, and Kyoko Ohno-Matsui

Department of Ophthalmology and Visual Science, Tokyo Medical and Dental University, Tokyo, Japan

Correspondence: Kyoko Ohno-Matsui, Department of Ophthalmology and Visual Science, Tokyo Medical and Dental University, 1-5-45 Yushima, Bunkyo-ku, Tokyo 1138510, Japan; k.ohno.oph@tmd.ac.jp.

PURPOSE. To identify structural abnormalities in the papillary and peripapillary area in eyes with pathologic myopia (PM) and normal IOP and to determine their relationship to visual field (VF) defects.

METHODS. One hundred eight eyes of 70 patients with PM were retrospectively studied. The disc-centered swept source optical coherence tomographic images and the Goldmann VF recorded within 1 year of the optical coherence tomographic examination were analyzed. Four structural abnormalities were identified: lamina cribrosa (LC) defects, ridge protrusions, intrachoroidal cavitations (ICC), and prelaminar schisis. The correspondence of the VF defects with the structural abnormalities was assessed.

RESULTS. The mean age, axial length, and optic disc area of the 108 eyes were 58.7 ± 10.0 years, 31.1 ± 2.4 mm, and 4.7 ± 2.2 mm², respectively. Eighty-five of the 108 eyes (78.7%) had at least one abnormality and 49.4% (42/85) had two or more abnormalities. LC defects, ridge protrusions, ICC, and prelaminar schisis were detected in 47.2%, 33.3%, 21.3%, and 30.6% of the eyes, respectively. VF defects at the corresponding areas of these structural abnormalities were seen in 63% of the eyes with LC defects, 39% of the eyes with ridge protrusions, and 21% of the eyes with ICC.

CONCLUSIONS. Four kinds of structural abnormalities with corresponding VF defects are commonly observed in the papillary and peripapillary region of eyes with PM. The presence of these abnormalities suggests a possibility of functional damage.

Keywords: pathologic myopia, visual field, optic disc, structural abnormalities

Myopia is a known risk factor for glaucoma, and the incidence of glaucoma and visual field (VF) defects is reported to be associated with high myopia.[1–3] Various optic disc-related anatomical structures, such as the entry point of the central retinal vessels, and optic disc rotation and tilt, were found to be associated significantly with the presence of myopia.[4] In addition, it has been reported that myopia causes systematic and location-specific shifts in the retinal nerve fiber layer (RNFL) thickness which results in myopia-specific thickness abnormality patterns.[5] Kang et al.[6] used the Cirrus HD OCT and found that the RNFL thickness was significantly affected by the ocular magnification owing to myopia. Moreover, myopes have a relatively decreased sensitivity in the paracentral and temporal VF areas, causing subtle but systematic changes in the relative light sensitivity over the entire VF, which interact with the glaucomatous vision loss.[7] Thus, high myopia and especially pathologic myopia (PM) are usually excluded from the studies evaluating glaucoma. However, VF defects caused by damage of the optic disc are relatively common in PM eyes.[8,9] Therefore, the detection of papillary and peripapillary damage is important in patients with PM.

Because the assessments of the circumpapillary RNFL and the optic disc morphology in early glaucomatous eyes are indecisive in PM eyes, VF tests have become more important. However, it is difficult to interpret the static VF test results accurately because of the presence of large peripapillary atrophy and coexisting myopic choroidal atrophy. Thus, Goldmann VF testing has been reported to be useful for analyzing the VF changes in PM eyes.[8] However, there has not been a study that precisely determined the relationship between the structural abnormalities and the VF defects in patients with PM.

Thus, the purpose of this study was to identify structural abnormalities occurring in papillary and peripapillary areas of PM eyes using swept-source OCT and to determine the correlation between the structural abnormalities and VF changes.

METHODS

The procedures used in this study conformed to the tenets of the Declaration of Helsinki and were approved by the

Ethics Committee of Tokyo Medical and Dental University. We reviewed the medical records of patients who visited the Advanced Clinical Center for Myopia between January 2018 and December 2020. A poster was displayed in the outpatient clinic to inform all the patients about the current study and instructions on how to opt-out of this study.

The inclusion criteria were (1) patients with PM, that is, with myopic maculopathy equal to or more serious than diffuse atrophy,[10] or with posterior staphylomas[11–13]; (2) eyes with disc-centered OCT examinations; and (3) eyes with Goldmann VF tests within 1 year of the OCT examination. Eyes with prior vitreoretinal surgery or laser treatment, with other diseases that can affect the VF, for example, optic neuritis and retinitis pigmentosa, with an IOP of greater than 21 mm Hg, or with poor-quality OCT images were excluded.

The fundus photograph of each eye was examined carefully for the typical signs of glaucoma. Eyes were excluded if any of the followings was presented: (1) a notch in the disc rim in the temporal inferior region or the temporal superior region; (2) a localized RNFL defect which could not be explained by any other cause than glaucoma; or (3) an abnormally large cup size when compared with the optic disc size.

Examinations

The age, sex, refractive error, best-corrected visual acuity, axial length, and IOP were collected from medical records. The disc size and the ratio of the vertical and horizontal disc diameters, the V/H disc ratio, were measured on the 50° fundus photographs (TRC-50DX, Topcon, Tokyo, Japan) using the built-in software (PDT/MPS software; Topcon) with modifications for axial lengths and refractive errors on the magnification. The presence of posterior staphylomas was determined by either the ultra-widefield OCT images or Optos fundus photographs as described elsewhere.[14–16]

Analyses of Structural Changes in Papillary and Parapapillary Areas in Disc-Centered OCT Images

Disc-centered swept-source OCT images (DRI-OCT Atlantis and DRI-OCT Triton, Topcon Co) were analyzed and measured with the built-in IMAGEnet software. The OCT scanning protocols included a scan length of 9 mm with 12 equal radial meridian scans centered on the optic disc. In addition, 5-line cross-scans and a disc-centered 3-dimentional volumetric scan covering an area of 6 × 6 mm² were also analyzed when available. We focused on four types of structural abnormalities: lamina cribrosa (LC) defects, ridge protrusions, intrachoroidal cavitation (ICC), and prelaminar schisis. The ridge protrusion is an anterior protrusion of the sclera temporal to the optic disc and was described as type IX staphyloma by Curtin.[17]

To avoid false-positive cases, the LC defects were required to be present in two neighboring radial line scan images. The location of the LC defects was classified as being in the superior, inferior, temporal, and nasal quadrants, which are outlined by two radial lines centered on the disc center at 45° to 225° and 135° to 315° (Supplementary Fig. S1A). The width of the LC defect in each quadrant was measured at the level of the LC where the widest LC defect was observed. The retinal thickness over the LC defect was measured perpendicularly to the estimated level of the inner surface of the LC at the site where the LC defect was present in the OCT image where the thinnest retina was observed (Supplementary Fig. S1D). The retinal thickness was measured instead of the RNFL thickness because the detection of RNFL was often difficult in thin and stretched retina of PM eyes.

The height of the ridge protrusion was defined as the distance between the plane of the most protruded point of the scleral inner surface and the plane of the scleral inner surface at disc margin (Supplementary Fig. S1B, S1C). The height should be more than 150 μm. The retinal thickness was measured both at the top of the ridge and on the slope between the top and the disc where the thinnest retinal tissue was present.

The site of the ICC was assigned to four quadrants in the same way as the LC defects. The retinal thickness at the margin of ICC was determined as the thinnest retinal thickness at the ICC margin which was measured perpendicularly from the retinal surface to the ICC border.

A prelaminar schisis is seen as a splitting of the tissue in the prelaminar optic disc in OCT images and has been reported to coexist with peripapillary retinoschisis in glaucomatous eyes.[18–20] Thus, the presence of prelaminar schisis and the coexistence of peripapillary retinoschisis were detected.

The correspondence in the locations of the VF defects and the structural abnormalities was analyzed for each patient by two masked authors (SX and KOM). Goldmann perimetry was performed with the refractive error fully corrected by disposable contact lenses. The VF was classified as abnormal if it contained one or more of the following findings: one or more scotomas with a minimum width of 5°, a horizontal nasal step in one isopter or the sum of steps of multiple isopters of at least 10°, or the presence of a sector-shaped defect as described in an earlier study.[21] The spatial correspondence between the structural abnormalities and the VF detects was determined by referring to the Garway–Heath map[22] and the geometry of the RNFL. A central or paracentral scotoma with coexisting macular atrophy were excluded from analyses. Eyes with a generalized constriction of the VF were excluded from analyses because determining a structure–function relationship was difficult.

Statistical Analyses

The descriptive parameters are reported as the means ± standard deviations. The significance of differences in the age, axial length, refractive error, best-corrected visual acuity, IOP, disc area, V/H disc ratio, and the retinal thickness over the structural abnormalities were determined by the Student t-test or the Mann–Whitney U test. The comparison on the width of the LC defects in the four quadrants was determined by Kruskal–Wallis tests. Pearson's χ^2 tests were used for comparisons of the sex distribution, the grades of myopic maculopathy, and for correlations between posterior staphylomas and structural abnormalities. Statistical analyses were performed with the SPSS software (version 22.0, IBM-SPSS, Chicago, IL). The generation and calculation of the receiver operating characteristic curve was performed with the R package. A P value of less than 0.05 (2-sided) was accepted as significant.

RESULTS

One hundred eight eyes of 70 patients (47 women, 23 men) were studied. Demographic data for the patients are shown in Table 1. Eighty-five of the 108 eyes (78.7%) had at least

TABLE 1. Comparison of the Clinical Characteristics Between Pathological Myopic Eyes With and Without Structural Abnormalities

	Total	LC Defect			Ridge			ICC			Prelaminar Schisis		
		Positive	Negative	P Value	Positive	Negative	P Value	Positive	Negative	P Value	Positive	Negative	P Value
Eyes	108	51 (47.2%)	57 (52.8%)	–	36 (33.3%)	72 (66.7%)	–	23 (21.3%)	85 (78.7%)	–	33 (30.6%)	75 (69.4%)	–
Age (years)	58.7 ± 10.0	57.1 ± 10.4	60.1 ± 9.5	0.159†	61.2 ± 9.2	57.5 ± 10.2	0.173†	60.3 ± 7.1	58.3 ± 10.6	0.566†	63.0 ± 8.4	56.8 ± 10.1	0.001†
Sex				0.553‡			0.021‡			0.600‡			0.345‡
Female	75	34	41		30	45		17	58		25	50	
Male	33	17	16		6	27		6	27		8	25	
SE (D)	–16.5 ± 4.5	–17.9 ± 4.4	–15.1 ± 4.2	0.008*	–16.9 ± 4.1	–16.4 ± 4.7	0.656*	–15.4 ± 3.5	–16.8 ± 4.7	0.291*	–15.9 ± 3.4	–16.8 ± 4.9	0.398*
AxL (mm)	31.1 ± 2.4	31.4 ± 2.3	30.9 ± 2.5	0.279*	32.4 ± 2.1	30.5 ± 2.3	<0.001*	30.2 ± 2.2	31.4 ± 2.4	0.016*	30.2 ± 1.8	31.5 ± 2.5	0.001*
BCVA (logMAR units)	0.3 ± 0.5	0.4 ± 0.5	0.2 ± 0.3	0.064†	0.3 ± 0.5	0.3 ± 0.4	0.273†	0.1 ± 0.3	0.3 ± 0.5	0.017†	0.3 ± 0.6	0.2 ± 0.4	0.897†
IOP (mm Hg)	14.6 ± 3.2	14.7 ± 3.8	14.5 ± 2.6	0.754*	14.6 ± 3.4	14.5 ± 3.1	0.937*	14.1 ± 3.4	14.7 ± 3.1	0.413*	15.4 ± 3.3	14.2 ± 3.1	0.063*
Disc area (mm²)	4.7 ± 2.2	5.5 ± 2.1	4.1 ± 2.1	0.001*	5.2 ± 1.9	4.5 ± 2.3	0.068*	4.0 ± 1.8	4.9 ± 2.2	0.065*	4.2 ± 1.6	4.9 ± 2.4	0.072*
V/H disc ratio	1.6 ± 0.4	1.4 ± 0.4	1.7 ± 0.4	<0.001*	1.7 ± 0.4	1.5 ± 0.4	0.010*	1.6 ± 0.4	1.6 ± 0.4	0.723*	1.5 ± 0.4	1.6 ± 0.4	0.442*
Myopic maculopathy				0.934‡			0.005‡			0.325‡			0.624‡
PDCA	19	8	11		0	19		5	14		6	13	
MDCA	48	24	24		18	30		12	36		17	31	
C3	25	12	13		12	13		5	20		7	18	
C4	16	7	9		6	10		1	15		3	13	
Staphyloma (+)	64 (59.3%)	30 (27.8%)	34 (31.5%)	0.931‡	34 (31.5%)	30 (27.8%)	<0.001‡	11 (10.2%)	53 (49.1%)	0.208‡	19 (17.6%)	45 (41.7%)	0.813‡
Staphyloma (–)	44 (40.7%)	21 (19.4%)	23 (21.3%)		2 (1.9%)	42 (38.9%)		12 (11.1%)	32 (29.6%)		14 (13.0%)	30 (27.8%)	

* Student t test.
† Mann–Whitney U test.
‡ χ² tests.
SE, spherical equivalence; AxL, axial length; BCVA, best-corrected visual acuity ; V/H disc ratio, the ratio between the vertical and horizontal disc diameter; PDCA, peripapillary diffuse choroidal atrophy; MDCA, macular diffuse choroidal atrophy; C3, patchy chorioretinal atrophy; C4, macular chorioretinal atrophy.

one of the four structural abnormalities. Different structural abnormalities were found in the same eye in 42 of the 85 eyes (49.4%) (Supplementary Fig. S2A). These four structural abnormalities were observed in eyes with a wide range of axial lengths and disc sizes (Supplementary Fig. S2B).

LC Defects

LC defects were observed in 51 of the 108 eyes (47.2%). Eyes with LC defects were significantly more myopic, had larger optic discs, and smaller V/H disc ratios than the eyes without LC defects (Table 1). LC defects were commonly observed in multiple quadrants (1.7 ± 0.8/eye; range, 1–3). The LC defect in 36 of the 51 eyes (70.6%) was located in the temporal quadrant (Fig. 1), 26 (51.0%) in the inferior quadrant (Fig. 2), 21 (41.2%) in the superior quadrant (Fig. 2), and 6 (11.8%) in the nasal quadrant, including overlaps.

The mean width of the LC defect was 282.8 ± 193.2 µm (median, 227 µm; range, 34–814 µm). There was no significant difference in the width of LC defects in different quadrants, although the nasal defects tended to be larger (Table 2).

The thickness of the thinnest retina over the LC defects was 135.2 ± 120.4 µm (median, 119 µm; range, 0–647 µm). There was no significant difference in the retinal thickness over the LC defects in different quadrants, although the overlying retina tended to be thicker over the nasal quadrant (Table 2).

Analyses of the VF showed that 32 eyes (62.7%) had corresponding VF defects. More specifically, 76.2% (16/21) of the superior LC defects (Fig. 2B), 57.7% (15/26) of the inferior LC defects (Fig. 2F), and 38.9% (14/36) of the temporal LC defects (Fig. 1) had corresponding VF defects. None of the nasal defects had corresponding VF defects. The differences in the width of the LC defect between groups with and without corresponding VF defects were not significant (243.3 ± 175.3 vs. 319.2 ± 195.9 µm; $P = 0.079$).

The retinal thickness over the LC defect was significantly thinner (52.2 ± 64.0 vs. 213.7 ± 107.4 µm; $P < 0.001$) in eyes with corresponding VF defects than in those without VF defects. The cut-off value of the retinal thickness over LC defects for VF defects was 136.5 µm, with a sensitivity of 89.5% and a specificity of 78.9% (area under the curve,
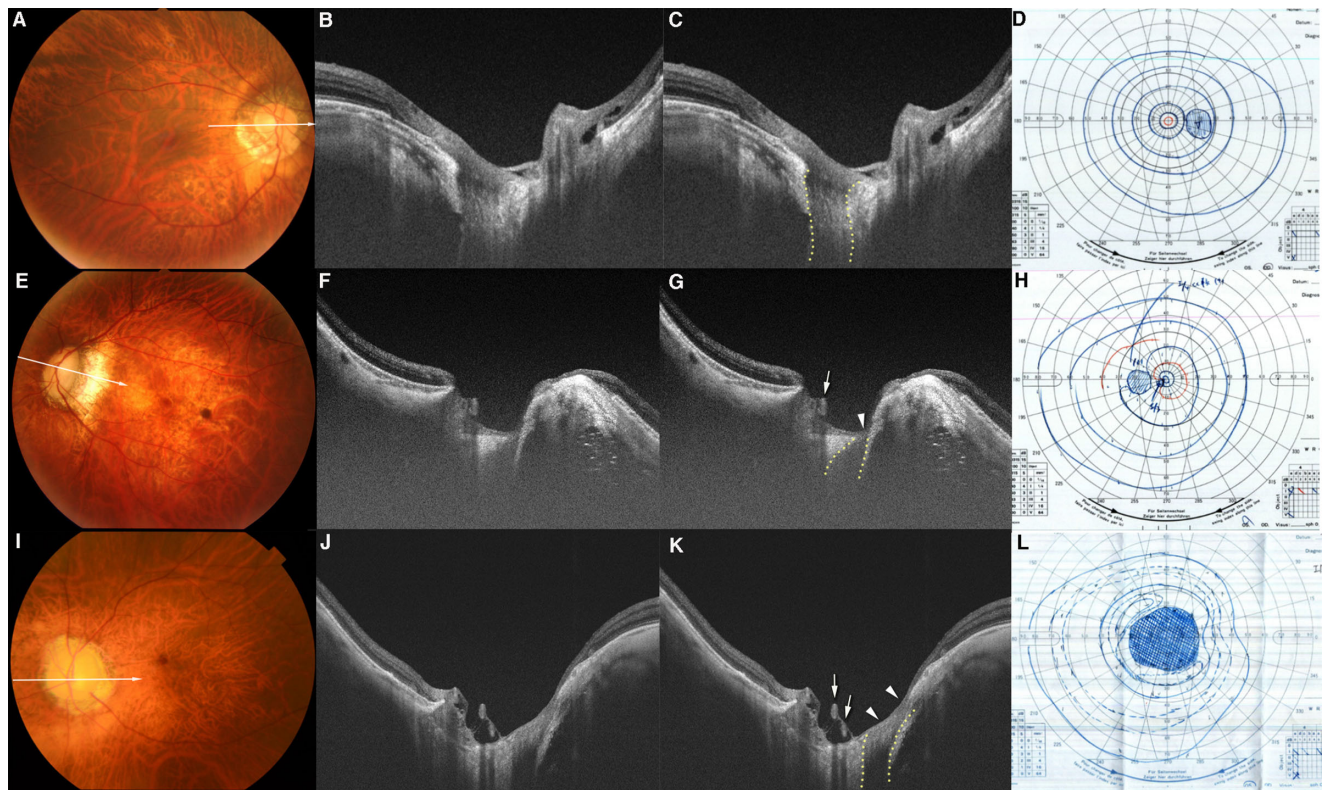

FIGURE 1. Temporal LC defects with and without corresponding VF defects. (**A**) Fundus photograph of the right eye of a 66-year-old woman with an axial length of 29.5 mm. The arrow indicates the OCT scan line in (**B**) and (**C**). (**B, C**) OCT image shows a decrease in the visibility of the LC on the temporal side (within *dotted lines* in **C**), which is classified as a LC defect. The width of temporal LC defect is 505 µm. The retinal tissue over the LC defect and in the peripapillary region remains thick. (**D**) Goldmann VF test shows a normal VF. (**E**) Fundus photograph of the left eye of a 50-year-old man with an axial length of 33.1 mm. The arrow indicates the OCT scan lines in (**F**) and (**G**). (**F, G**) OCT image shows LC defects on the temporal side (within *dotted lines* in **G**). The LC defects are deep and have a flask-neck shape with the anterior part narrower and wider than the posterior part. The retina overlying the LC defect is thin (*arrowhead* in **G**). Retinal vessels protruding anteriorly can be seen to shift toward the opposite side from the site of the LC defects (*arrow* in **G**). A ridge protrusion is seen as a scleral protrusion anterior and temporal to the optic disc. The retina is thin at the top and on the slope of the ridge. (**H**) VF shows a relatively small scotoma in the paracentral field. I. Fundus photograph of the left eye of a 66-year-old man with an axial length of 27.1 mm. No macular atrophy is seen. The arrow indicates the OCT scan line in (**J**) and (**K**). (**J, K**) OCT image shows a wide LC defect on the temporal side (within the *dotted lines* in **K**). The width of this LC defect is 786 µm. The retina overlying the LC defect is extremely thin and almost absent (*arrowheads* in **K**). Anteriorly protruding retinal vessels can be seen (*arrows* in **K**). L. VF shows central scotoma.
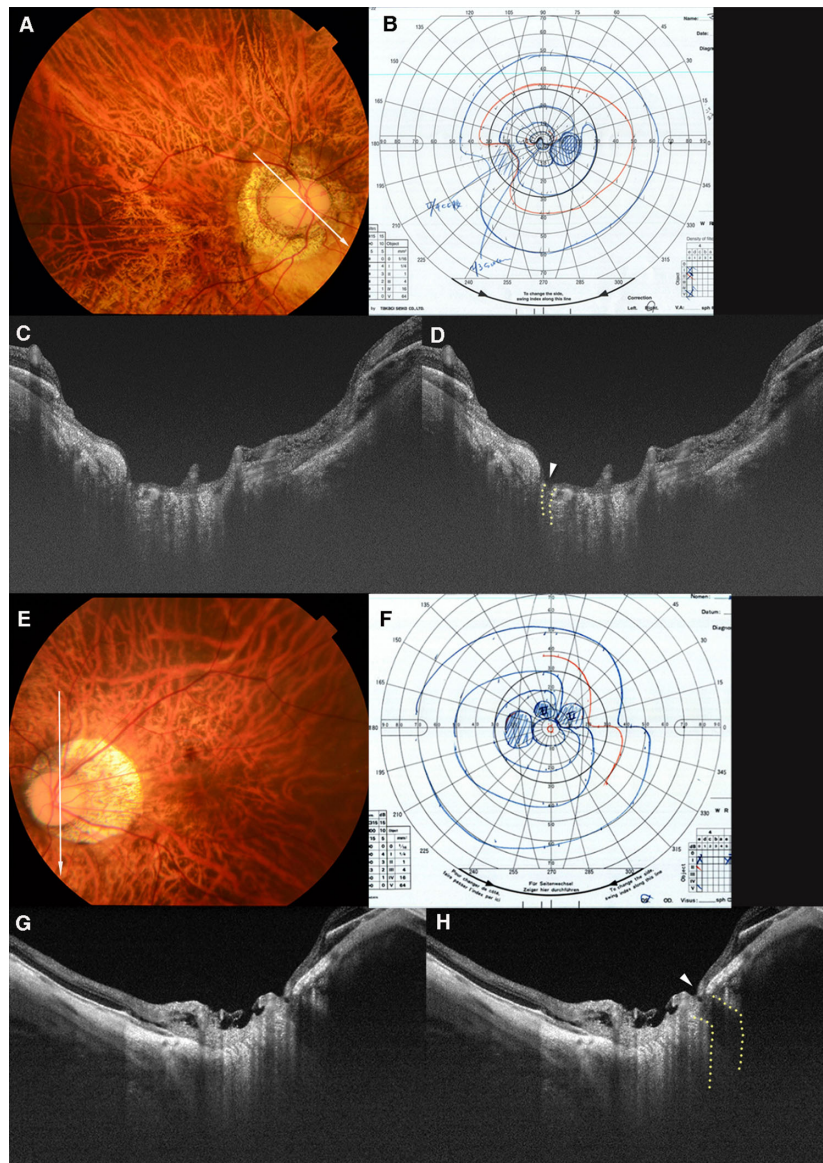
FIGURE 2. LC defects in superior and inferior quadrants with corresponding VF defects. (**A**) Fundus photograph of the right eye of a 55-year-old woman with an axial length of 31.2 mm. The arrow indicates the OCT scan line in (**C**) and (**D**). (**B**) Defect of the inferior–nasal VF is seen in the Goldmann VF. (**C**, **D**) OCT image shows a cleft-like LC defect in the superior margin of the optic disc (*dotted line* in **D**). A nearly total loss of the nerve fiber layer (*arrowhead* in **D**) over the LC defect can be seen. The LC defect and nerve fiber layer loss correspond to the inferior–nasal VF defect. (**E**) Fundus photograph of the left eye of a 39-year-old man with an axial length of 30.0 mm. The arrow indicates the OCT scan line in (**G**) and (**H**). (**F**) A nasal step in the superior VF can be seen. There are no VF defects in the inferior field. (**G**, **H**) OCT image shows a disinsertion of the LC from the peripapillary scleral flange in the inferior region (outlined by dotted line in **H**). A thinning of the retinal tissue over the defect can be seen (*arrowhead* in **H**).

0.9134; 95% confidence interval, 0.8537–0.9732), based on the receiver operating characteristic curve.

Ridge Protrusion

Ridge protrusion was observed in 36 of the 108 eyes (33.3%). Patients with ridge protrusion were more likely to be women with a longer axial length, a larger V/H disc ratio, and a more severe grade of myopic maculopathy. Posterior staphyloma was present in 94.4% of the eyes with ridge protrusion (Table 1). The retina was thin, especially on the slope between the disc and the top of the ridge (Fig. 3). The thinnest retina varied from 0 (unable to detect) to 194 µm.

Overall, the retina at the top of the ridge was only slightly thicker than the thinnest retina on the slope.

Among the 36 eyes with ridge protrusion, 21 eyes (58.3%) also had LC defects (Figs. 3B, 3E) and 15 were detected in the temporal, 13 in the inferior, 8 in the superior, and 1 in the nasal quadrants. Conus pits were found in 14 of the 36 eyes (38.9%) with ridge (Fig. 3H) which was significantly more than the 4 of the 72 eyes (5.6%) without ridge ($P < 0.001$).

Among the 36 eyes with ridge, 14 eyes (38.9%) had corresponding VF defects. The retinal thickness on the slope of the ridge was significantly thinner in these 14 eyes with corresponding VF defects than that in the remaining eyes (44.2 ± 33.5 vs. 81.0 ± 37.4 µm; $P = 0.004$). In these

TABLE 2. Width of the LC Defects and Retinal Thickness Over the LC Defects in Different Regions

Region	Eyes With LC Defects (n)	Width of LC Defects, Mean ± SD (µm)	Retinal Thickness Over LC Defects, Mean ± SD (µm)
Total	89[*] (including overlap)	282.8 ± 193.2	135.2 ± 120.4
Superior	21	244.2 ± 172.7	104.3 ± 169.3
Temporal	36	303.4 ± 191.0	136.4 ± 92.9
Inferior	26	226.7 ± 137.7	141.4 ± 127.7
Nasal	6	468.8 ± 314.8	189.7 ± 63.8
P value[†]	-	0.18	0. 05

SD, standard deviation.

[*] The total number of the quadrants presented with LC defects.

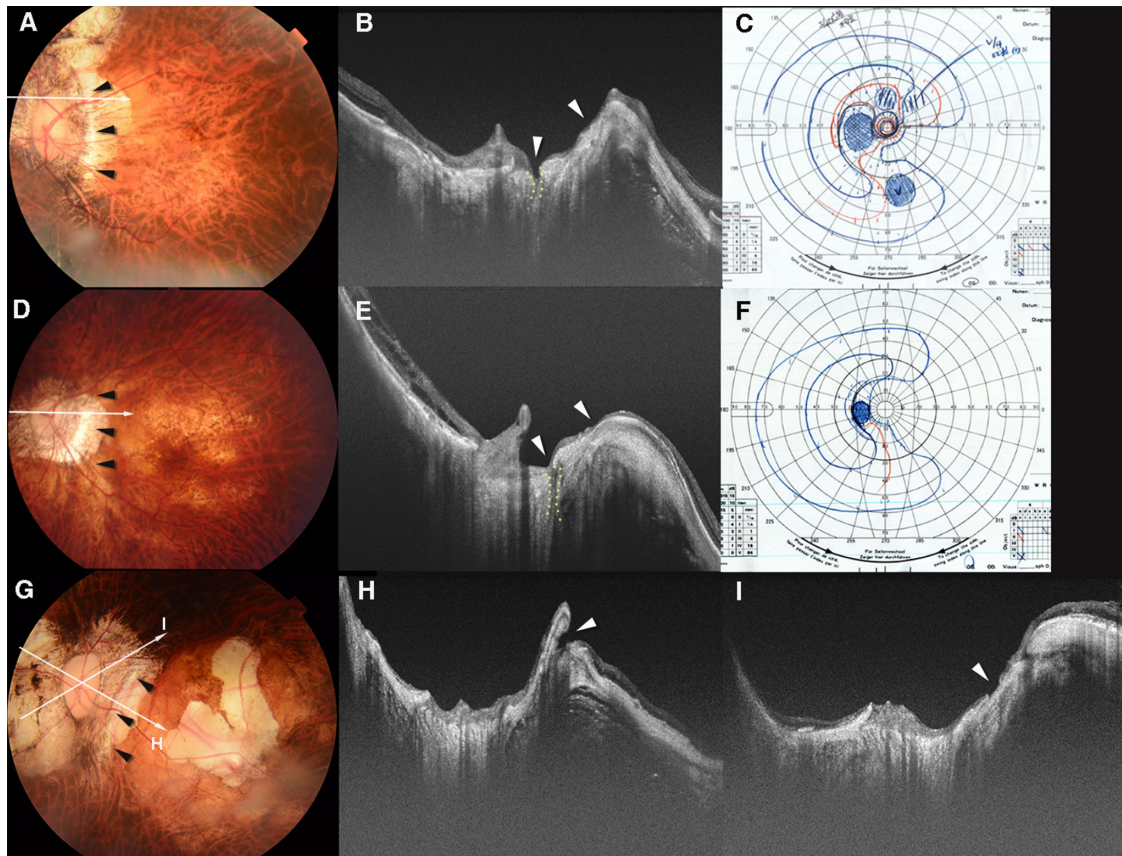[†] Independent samples Kruskal-Wallis test.

FIGURE 3. Scleral ridge protrusion temporal to the optic nerve and coexisting lesions. (**A**) Fundus photograph of the left eye of a 52-year-old woman with an axial length of 32.1 mm. The *arrowheads* temporal to the disc point to the ridge. Arrow indicates the OCT scan line in (**B**). (**B**) OCT image shows a high ridge temporal to the optic nerve. The height of the ridge is 459 µm. A defect (within *dotted lines*) in the LC can be seen in the superior region of the optic disc. Retinal tissue is almost absent from near the top of the ridge to the LC defect (*arrowheads*). (**C**) VF shows a scotoma in the inferior area. Relative scotomas are also seen in the upper VF. (**D**) Fundus photograph of the left eye of a 69-year-old woman with an axial length of 30.9 mm. The *arrowheads* show a ridge temporal to the optic disc. Arrow indicates the OCT scan line in (**E**). (**E**) OCT image shows a ridge protrusion temporal to the optic disc with the coexistence of a narrow LC defect (within *dotted lines*). The height of the ridge is 394 µm. The retinal tissue is thinned on both sides of the slopes of the ridge and over the LC defect (*arrowheads*). (**F**) A VF defect extending from the center to the nasal field. (**G**) A fundus photograph of the left eye of a 59-year-old woman with an axial length of 36.7 mm. The *arrowheads* show a ridge temporal to the disc. The arrows indicate the OCT scan lines in (**H**) and (**I**). An irregularly shaped macular atrophy is present. (**H**) OCT image shows a high ridge temporal to the optic disc. The height of the ridge is 737 µm. A large conus pit is observed near the peak of the ridge along the slope between the ridge and the macula (*arrowhead*). (**I**) OCT image shows a shallow scleral break with discontinuity of the overlying retinal tissue (*arrowhead*) in the superior peripapillary area. The correspondence of the scleral defects was not compared with the VF defects because of coexisting macular atrophy.

14 eyes, 6 eyes had a loss of retinal tissue over the conus pit (Fig. 3H) and 6 eyes had a coexistence of retinal thinning over the LC defect (Figs. 3B, 3E). In the other two eyes without LC defects or conus pits, the mean retinal thickness on the slope of the ridge was 52 and 57 µm, respectively.
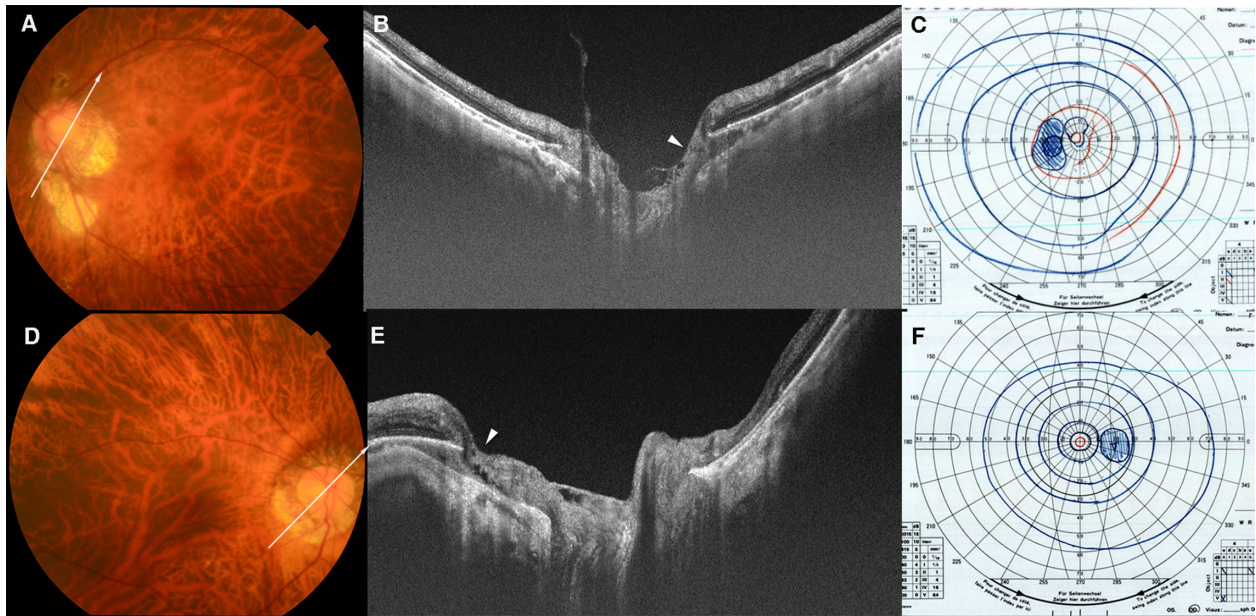
FIGURE 4. ICC without VF defects. (**A**) A fundus photograph of the left eye of a 58-year-old woman with an axial length of 28.7 mm. An irregular-shaped parapapillary atrophic (PPA) area is seen. The arrow indicates the OCT scan line in (**B**). (**B**) OCT image shows the ICC above and beneath the optic disc. The retinal tissue is relatively normal at the ICC margin (*arrowhead*), except for a slight prelaminar retinoschisis closer to the disc center. This retinoschisis is probably caused by vitreous traction. (**C**) VF shows no obvious defect in the upper and lower field. An enlargement of the blind spot owing to the PPA can be seen. (**D**) Fundus photograph of the right eye of a 66-year-old woman with an axial length of 29.5 mm. The arrow indicates the OCT scan line in (**E**). (**E**) OCT image shows ICC below and temporal to the optic disc. The overlying retina appears to be herniated toward the ICC space (*arrowhead*) and retinoschisis is seen near the ICC margin. However, no retinal defect can be seen at the ICC margin. (**F**) VF shows no obvious changes.

Intrachoroidal Cavitation

An ICC was observed in 23 eyes (21.3%), and these eyes had significantly shorter axial length and better best-corrected visual acuity than the eyes without ICC (Table 1). The ICC was mostly located inferior to the optic disc (91.3%), and in the superior (43.5%), nasal (43.5%), and temporal (17.4%) quadrants (Figs. 4 to 6). Six eyes (26.1%) had almost no retina at the margin of ICC and another three eyes had a retinal thinning to less than 50 μm at the margin (Fig. 5).
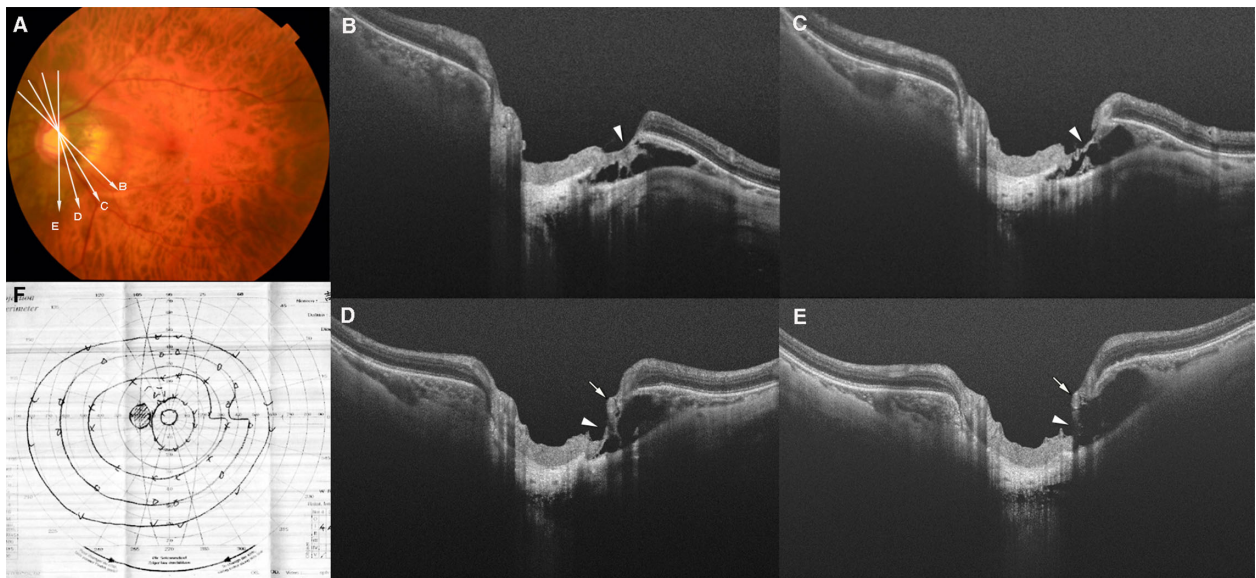

FIGURE 5. ICC with VF defects. (**A**) Fundus photograph of the left eye of a 64-year-old man with axial length of 28.4 mm. The arrows indicate the OCT scan lines in (**B–E**). (**B–E**) Serial OCT images showing relatively deep ICC with fluid space inferior to the optic disc. The retinal tissue over the ICC is extremely thinned and stretched across the ICC (*arrowheads* in **B–E**). A retinal vessel can be seen to protrude slightly anteriorly (*arrows* in **D**, **E**). A full-thickness defect of the retina is observed next to this retinal vessel (**E**). (**F**) The VF shows superior nasal step that corresponds with the lower temporal ICC.
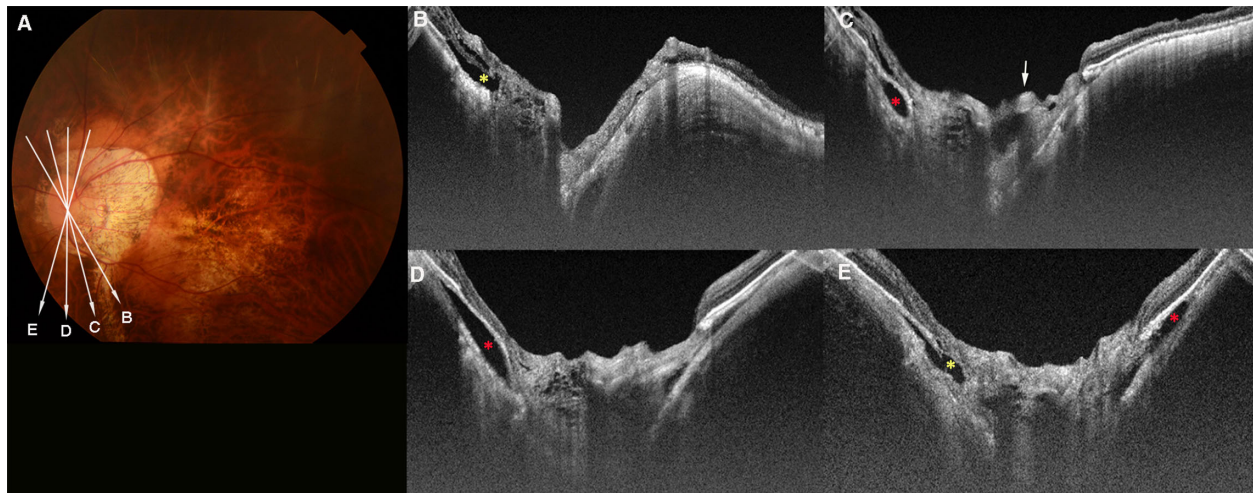
Figure 6. Prelaminar schisis coexisting with ICC in an eye with PM. (**A**) A fundus photograph of the left eye of a 67-year-old woman with axial length of 29.9 mm. The arrows indicate the OCT scan lines in (**B–E**). (**B–E**) OCT images showing a meshwork-like prelaminar schisis in a wide area within the disc. A cross-section of an anteriorly protruding retinal vessel can be seen (*arrow* in **C**). Peripapillary retinoschisis and retinal detachment (*yellow asterisks* in **B** and **E**) can be seen in the superior region. Hypo-reflective area under the RPE (*red asterisks* in **C–E**), suggesting the presence of an ICC can also be seen.

Five eyes (20.8%) with ICC had corresponding VF defects (Fig. 5) in either the superior (two eyes) or the inferior (three eyes) quadrant. Three of these 5 eyes had almost no retina at the ICC margin, and the remaining two eyes had a retina thinner than 50 µm at the margin.

Prelaminar Schisis

A prelaminar schisis was observed in 33 eyes (30.6%), and the patients with these eyes were significantly older and had significantly shorter axial length (Table 1). Nine of the 33 eyes (27.3%) had additional retinoschisis in the peripapillary area, and 9 other eyes (27.3%) had both peripapillary retinoschisis and peripapillary retinal detachment (Figs. 6 and 7).

Two causes for the prelaminar schisis are suggested from the OCT images. The most common finding was a stretching and hanging of the retinal vessels anteriorly which was observed in 27 eyes (81.8%) (Figs. 6 and 7). Vitreous or epiretinal proliferation-related schisis was observed in six eyes (18.2%). The VFs for this abnormality were not analyzed because the spatial relationships were difficult to detect.

DISCUSSION

Unlike nonmyopic glaucomatous eyes, whose key feature is the loss of retinal ganglion axons within the LC,[23] the structural abnormalities in PM eyes were diverse and commonly coexisted. Figure 8 illustrates each type of these abnormalities.

LC Defects in PM Eyes

Earlier studies showed that the incidence of LC defects in glaucomatous eyes, either with or without myopia, varied from 6.6% to 42.9%.[24–26] In our PM eyes, the prevalence of LC defects was considerably higher at 47.2%. In nonmyopic glaucomatous eyes, LC defects exist exclusively in the inferior and superior regions.[26,27] In our patients with PM, the temporal LC defect was the most common type. The same finding was reported by Sawada et al, showing large pores in the temporal LC in myopic eyes without glaucoma, although extreme myopia (refractive error of >10 D or an axial length of >28.5 mm) were excluded from their study.[28]

The width of the LC defects ranged from 34 to 814 µm. Two previous studies on glaucoma patients reported the width of the LC defects ranging from 101 to 267 µm.[25,27] Thus, the width of the LC defects in PM eyes varied considerably.

Our results indicated that it was not the width of LC defects, but rather the thinning of the retina over the LC defects that was correlated with the VF defects. The cut-off value of the retinal thickness had a high sensitivity and specificity. This result supported the concept that structural changes were associated with the functional abnormality in PM eyes as well. Considering that peripapillary retinal nerve fiber thickness is difficult to measure in PM eyes, the retinal thickness over the LC defects may be an important marker for VF defects in the clinical management of patients with PM.

Ridge Protrusions Temporal to the Optic Disc in PM Eyes

Eyes with ridge had more severe grades of myopic maculopathy and more than 90% of the eyes had a posterior staphyloma, suggesting that the ridge tended to be found in more severe forms of PM.

Although the relationship between the ridge protrusion and VF defects has been reported,[8] the reason for this relationship was not determined. We found that the ridge was frequently accompanied with conus pits and temporal LC defects. These structural abnormalities can develop either independently or simultaneously, but it seems that they may enhance the overall effect on the retinal tissue when they coexist. In addition, two eyes with ridge had VF defects without other abnormalities, which suggested that the presence of ridge alone may cause retinal thinning and may be an
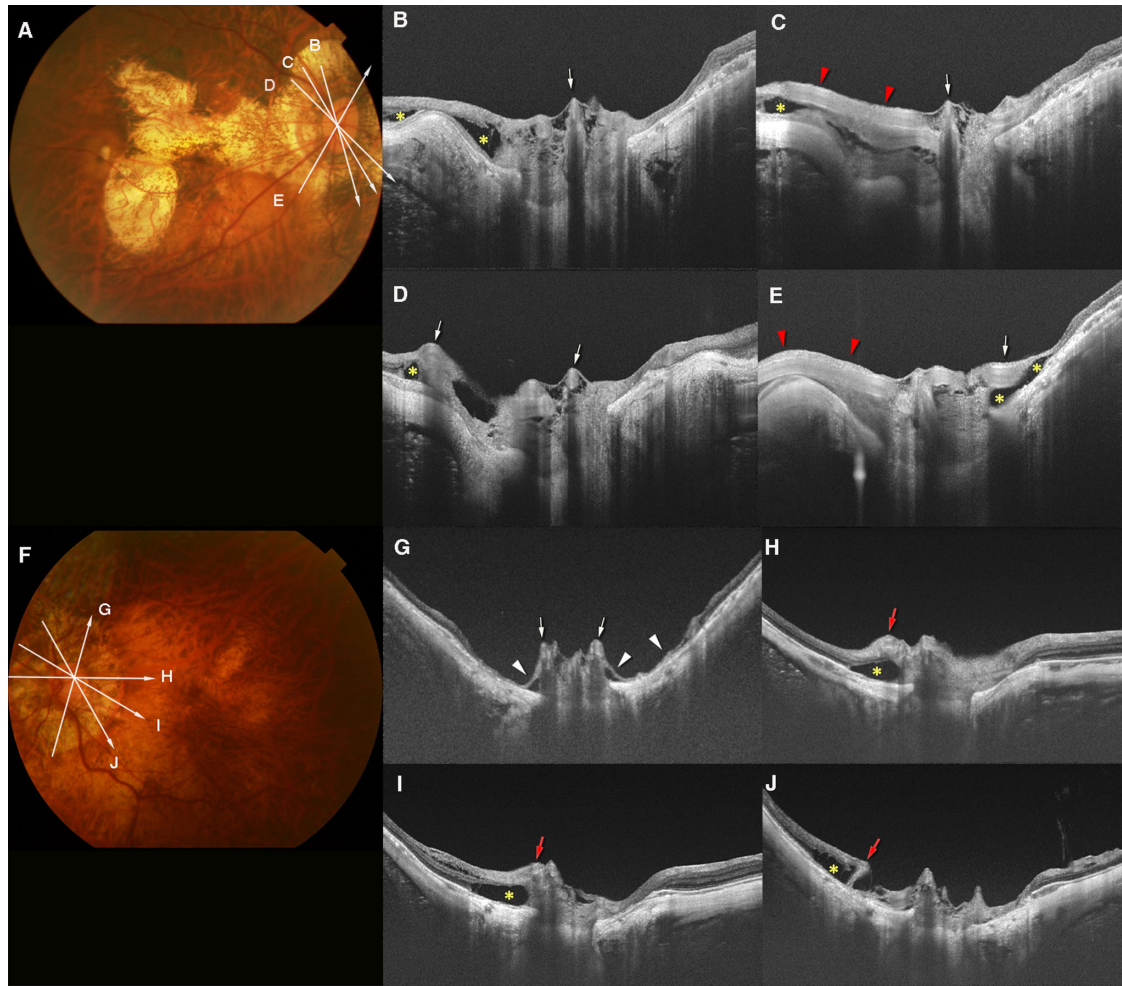
FIGURE 7. Prelaminar schisis and anterior protrusion of retinal vessels. (**A**) A fundus photograph of the right eye of a 66-year-old woman with an axial length of 30.2 mm. The arrows indicate the OCT scan lines in (**B–E**). (**B–E**) Prelaminar schisis is observed as a meshwork structure within the optic disc. Retinal vessels (*arrows* in **B–E**) within and around the optic disc are protruded anteriorly. Prelaminar schisis is obvious around the protruding retinal vessels. Peripapillary retinoschisis (*yellow asterisks*) is also seen. (**C, E**) Longitudinal course of the retinal vessels (*red arrowheads*) in the peripapillary region can be seen. (**F**) Fundus photograph of the left eye of a 61-year-old woman with an axial length of 31.2 mm. The arrows indicate the OCT scan line in (**G–J**). (**G–J**) Prelaminar schisis can be seen within the optic disc area. (**G**) Retinal vessels (*arrows*) are protruded anteriorly, and the retinal tissue around these protruded vessels is extremely thin (*arrowheads*) and detached from the sclera. (**H–J**) Peripapillary retinal vessels also protrude (leftmost *red arrows* in each image). Retinoschisis (*yellow asterisks*) is seen around these protruded vessels.

indicator of the fragility of the retina, which would make it more susceptible to damage and VF defect. Because the ridge can be easily detected in fundus photographs, it may be a convenient indicator for possible functional damage in clinical settings.

ICC in PM Eyes

ICC is reported to be present in 4.9% to 16.9% of highly myopic eyes.[29–31] One study reported glaucomatous VF defect in 71.0% of highly myopic eyes with ICC.[30] In our cohort, we found ICC in 21.3% of eyes with PM, and only 20% of the eyes with ICC had corresponding VF defects. Spaide et al.[32] reported a full-thickness retinal defect caused by the herniation of the retinal tissue into the posteriorly bowed sclera at the ICC margin. This finding is similar to the retinal thinning observed in our study. Thus, local retinal herniation and eventual tissue loss, instead of the presence of ICC itself, may be an important cause of the VF defects

and should be paid attention to during the clinical examinations of PM eyes.

Prelaminar Schisis in PM Eyes

Two recent studies reported the presence of prelaminar schisis in eyes with suspected or advanced glaucoma at a percentage of 41.4% and 44.6%, respectively.[18,20] In our cohort, prelaminar schisis was present in 30.6% of the PM eyes. We believe this finding is important in highly myopic eyes. However, because other structural abnormalities coexisted with prelaminar schisis, the association between prelaminar schisis and VF defects needs further studies.

Approximately 80% of the prelaminar schisis appeared to be caused by a stretching and hanging of the retinal vessels anteriorly, which is consistent with the report by Lowry et al.[18] Although the vitreous traction theory has been suggested for the development of peripapillary retinoschi-
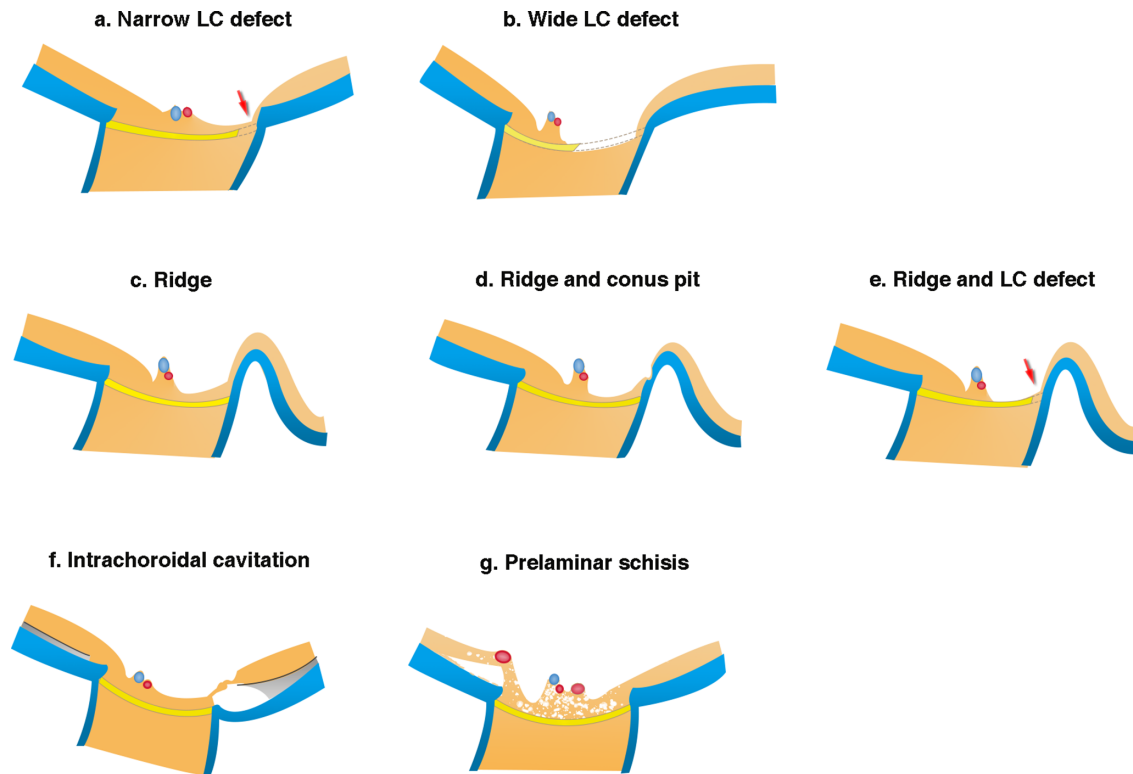
FIGURE 8. Schematic drawing showing the different structural abnormalities in PM eyes. (**a**) Narrow LC defect (*arrow*) is observed as a pit or disinsertion of the LC. In some cases, the defect is deep and continues up to areas posterior to the LC. The overlying retina is thin, and in some cases almost absent. Surrounding retinal tissue gradually thins toward the site of LC defects. (**b**) A wide LC defect seems to extend up to one-half the LC width with obvious thinning of the prelaminar tissue. In eyes with very wide LC defects, the central trunk of the retinal vessels tends to shift toward the opposite side from the site of LC defects. (**c**) Ridge is an anterior protrusion of the sclera temporal to the optic disc. Retinal thinning is marked on the slope between disc margin and the ridge peak. (**d**) Ridge protrusion and conus pit commonly coexist, and the retinal tissue over the conus pit is extremely thin and almost absent. (**e**) Ridge and LC defect can coexist, and the retinal tissue is obviously thin on the slope of ridge and over the LC defect (*arrow*). (**f**) ICC with large area of fluid space. The overlying retinal tissue bridging the ICC can be extremely stretched and thinned. (**g**) Prelaminar schisis is mainly caused by the retinal vessels on the disc hanging anteriorly. Retinoschisis is also seen around the anteriorly protruded retinal vessels in the peripapillary area.

sis in glaucomatous eyes,[20,33] the findings in our patients seemed to be more closely related to the inward traction by the retinal vessels. Interestingly, peripapillary retinoschisis and retinal detachment coexisted with prelaminar schisis in 54.5% of the eyes. The coexistence of peripapillary retinal detachment has not been reported, and the rate of coexistence of retinoschisis was much lower in non-PM glaucomatous eyes at 4.2% in the study by Sung et al.[20]

Indications of Structural Abnormalities in Non-PM Eyes

These findings suggest that the causes of the VF defects in PM eyes may be multifactorial, and the incidence may be underestimated. Because myopia can progress for a long time, the influence of these structural abnormalities on the visual function may occur at an earlier stage and continued to worsen before being identified.

The ridge protrusions and conus pits appear to be unique to PM eyes, and they should be paid attention to during the clinical examinations. In contrast, LC defects and prelaminar schisis also occur in nonmyopic eyes, but they may cause more serious damage in PM eyes. The investigation of these

two abnormalities in PM eyes may give clues for future studies in nonmyopic glaucomatous eyes.

Limitations

This study has several limitations. First, this study was hospital based, and the inclusion criteria were limited to patients who had undergone Goldmann VF testing. Although Goldmann VF is performed routinely at the Advanced Clinical Center for Myopia, there may be a significant selection bias in the population with PM. Second, we mainly used radial OCT scans to detect the structural abnormalities. Because the optic disc shape in eyes with PM varied considerably and the radial scans cannot provide a continuous segmentation of the structure, there may be some abnormalities missed during the analysis. Third, the exclusion criteria for typical glaucomatous change were based on disc appearance in fundus photographs. Because the coexisting peripapillary lesions like ICC and myopic fundus lesions are common in PM eyes, it is difficult to determine glaucoma solely based on VF examinations. Although eyes with normal IOP and with typical glaucomatous disc appearance were excluded, glaucoma may partly contribute to the structural and VF changes in some eyes. Fourth, a specific VF defect may be due to a combination of multiple structural changes, especially the

structural abnormalities we observed to coexist commonly. However, we have tried to identify the main cause of the local VF defects by comparing the degree of retinal tissue loss induced by each abnormality. Last, we measured the thinnest retinal thickness at each structural abnormalities because the measurement of RNFL is difficult in PM eyes. And the measurement of retinal thickness in these eyes may be affected by test–retest variability. Although we found that the retinal thinning over the LC defects is a good indicator for VF defect, further study is needed to determine and verify the cut-off value.

In conclusion, structural abnormalities in papillary and peripapillary areas were found in 78% of the PM eyes. The status of the retina overlying these abnormalities rather than the abnormalities seemed to be related to the VF defects. Various abnormalities often coexisted, suggesting that VF defects in PM eyes tended to be multifactorial. VF defects in PM eyes are difficult to suspect and thus may be overlooked and underestimated. Our results provide important clues on the pathogenesis and VF impairments in PM eyes.

References

1. Marcus MW, de Vries MM, Junoy Montolio FG, Jansonius NM. Myopia as a risk factor for open-angle glaucoma: a systematic review and meta-analysis. *Ophthalmology*. 2011;118:1989–1994.e1982.
2. Czudowska MA, Ramdas WD, Wolfs RC, et al. Incidence of glaucomatous visual field loss: a ten-year follow-up from the Rotterdam Study. *Ophthalmology*. 2010;117:1705–1712.
3. Cedrone C, Mancino R, Ricci F, Cerulli A, Culasso F, Nucci C. The 12-year incidence of glaucoma and glaucoma-related visual field loss in Italy: the Ponza eye study. *J Glaucoma*. 2012;21:1–6.
4. Baniasadi N, Wang M, Wang H, Mahd M, Elze T. Associations between optic nerve head-related anatomical parameters and refractive error over the full range of glaucoma severity. *Transl Vis Sci Technol*. 2017;6:9.
5. Elze T, Baniasadi N, Jin Q, Wang H, Wang M. Ametropia, retinal anatomy, and OCT abnormality patterns in glaucoma. 1. Impacts of refractive error and interartery angle. *J Biomed Opt*. 2017;22:1–11.
6. Kang SH, Hong SW, Im SK, Lee SH, Ahn MD. Effect of myopia on the thickness of the retinal nerve fiber layer measured by Cirrus HD optical coherence tomography. *Invest Ophthalmol Vis Sci*. 2010;51:4075.
7. Choi EY, Wong RCS, Thein T, et al. The effect of ametropia on glaucomatous visual field loss. *J Clin Med*. 2021;10:2796.
8. Ohno-Matsui K, Shimada N, Yasuzumi K, et al. Long-term development of significant visual field defects in highly myopic eyes. *Am J Ophthalmol*. 2011;152:256–265.e251.
9. Nagaoka N, Jonas JB, Morohoshi K, et al. Glaucomatous-type optic discs in high myopia. *PLoS One*. 2015;10: e0138825.
10. Ohno-Matsui K, Kawasaki R, Jonas JB, et al. International photographic classification and grading system for myopic maculopathy. *Am J Ophthalmol*. 2015;159:877–883.
11. Ohno-Matsui K, Lai T, Lai C-C, Cheung C. Updates of pathologic myopia. *Prog Retin Eye Res*. 2016;52:156–187.
12. Ohno-Matsui K, Wu P-C, Yamashiro K, et al. IMI pathologic myopia. *Invest Ophthalmol Vis Sci*. 2021;62:5.
13. Flitcroft DI, He M, Jonas JB, et al. IMI – defining and classifying myopia: a proposed set of standards for clinical and epidemiologic studies. *Invest Ophthalmol Vis Sci*. 2019;60:M20.
14. Shinohara K, Shimada N, Moriyama M, et al. Posterior staphylomas in pathologic myopia imaged by widefield optical coherence tomography. *Invest Ophthalmol Vis Sci*. 2017;58:3750–3758.
15. Ohno-Matsui K, Jonas JB. Posterior staphyloma in pathologic myopia. *Prog Retin Eye Res*. 2019;70:99–109.
16. Ohno-Matsui K. Proposed classification of posterior staphylomas based on analyses of eye shape by three-dimensional magnetic resonance imaging and wide-field fundus imaging. *Ophthalmology*. 2014;121:1798–1809.
17. Curtin BJ. The posterior staphyloma of pathologic myopia. *Trans Am Ophthalmol Soc*. 1977;75:67–86.
18. Lowry EA, Mansberger SL, Gardiner SK, et al. Association of optic nerve head prelaminar schisis with glaucoma. *Am J Ophthalmol*. 2021;223:246–258.
19. Fortune B. Pulling and tugging on the retina: mechanical impact of glaucoma beyond the optic nerve head. *Invest Ophthalmol Vis Sci*. 2019;60:26–35.
20. Sung MS, Jin HN, Park SW. Clinical features of advanced glaucoma with optic nerve head prelaminar schisis Prelaminar schisis in advanced glaucoma. *Am J Ophthalmol*. 2021;232:17–29.
21. Chauhan BC, Drance SM, Douglas GR. The use of visual field indices in detecting changes in the visual field in glaucoma. *Invest Ophthalmol Vis Sci*. 1990;31:512–520.
22. Garway-Heath DF, Poinoosawmy D, Fitzke FW, Hitchings RA. Mapping the visual field to the optic disc in normal tension glaucoma eyes. *Ophthalmology*. 2000;107:1809–1815.
23. Burgoyne CF, Downs JC, Bellezza AJ, Suh JK, Hart RT. The optic nerve head as a biomechanical structure: a new paradigm for understanding the role of IOP-related stress and strain in the pathophysiology of glaucomatous optic nerve head damage. *Prog Retin Eye Res*. 2005;24:39–73.
24. Takayama K, Hangai M, Kimura Y, et al. Three-dimensional imaging of lamina cribrosa defects in glaucoma using swept-source optical coherence tomography. *Invest Ophthalmol Vis Sci*. 2013;54:4798.
25. Han JC, Choi JH, Park DY, Lee EJ, Kee C. Border tissue morphology is spatially associated with focal lamina cribrosa defect and deep-layer microvasculature dropout in open-angle glaucoma. *Am J Ophthalmol*. 2019;203:89–102.
26. You JY, Park SC, Su D, Teng CC, Liebmann JM, Ritch R. Focal lamina cribrosa defects associated with glaucomatous rim thinning and acquired pits. *JAMA Ophthalmol*. 2013;131:314–320.
27. Tatham AJ, Miki A, Weinreb RN, Zangwill LM, Medeiros FA. Defects of the lamina cribrosa in eyes with localized retinal nerve fiber layer loss. *Ophthalmology*. 2014;121:110–118.
28. Sawada Y, Araie M, Ishikawa M, Yoshitomi T. Multiple temporal lamina cribrosa defects in myopic eyes with glaucoma and their association with visual field defects. *Ophthalmology*. 2017;124:1600–1611.
29. Shimada N, Ohno-Matsui K, Nishimuta A, Tokoro T, Mochizuki M. Peripapillary changes detected by optical

coherence tomography in eyes with high myopia. *Ophthalmology*. 2007;114:2070–2076.

30. Shimada N. Characteristics of peripapillary detachment in pathologic myopia. *Arch Ophthalmol*. 2006;124:46.

31. You QS, Peng XY, Chen CX, Xu L, Jonas JB. Peripapillary intrachoroidal cavitations. The Beijing Eye Study. *PLoS One*. 2013;8:e78743.

32. Spaide RF, Akiba M, Ohno-Matsui K. Evaluation of peripapillary intrachoroidal cavitation with swept source and enhanced depth imaging optical coherence tomography. *Retina*. 2012;32:1037–1044.

33. Grewal DS, Merlau DJ, Giri P, et al. Peripapillary retinal splitting visualized on OCT in glaucoma and glaucoma suspect patients. *PLoS One*. 2017;12:e0182816.